Journal of Materials Chemistry B

Accepted Manuscript

This is an *Accepted Manuscript*, which has been through the Royal Society of Chemistry peer review process and has been accepted for publication.

Accepted Manuscripts are published online shortly after acceptance, before technical editing, formatting and proof reading. Using this free service, authors can make their results available to the community, in citable form, before we publish the edited article. We will replace this *Accepted Manuscript* with the edited and formatted *Advance Article* as soon as it is available.

You can find more information about *Accepted Manuscripts* in the Information for Authors.

Please note that technical editing may introduce minor changes to the text and/or graphics, which may alter content. The journal's standard Terms & Conditions and the Ethical guidelines still apply. In no event shall the Royal Society of Chemistry be held responsible for any errors or omissions in this *Accepted Manuscript* or any consequences arising from the use of any information it contains.

ROYAL SOCIETY OF CHEMISTRY

www.rsc.org/materialsB

Journal of Material Chemistry RSCPublishing

ARTICLE

Organic Nanoparticles Composed of Fréchet-type Dendrons: Synthesis, Characterization, Self-assembly and Reversible Guest Encapsulation

Cite this: DOI: 10.1039/x0xx00000x

Received ooth January 2012,
Accepted ooth January 2012

DOI: 10.1039/x0xx00000x

www.rsc.org/

Sreedevi Krishnakumar and Karical R. Gopidas *

Novel organic nanoparticles composed of Fréchet-type dendrons have been synthesized by a simple one-pot reaction, which involved etching off the gold core in a first generation gold nanoparticle-cored dendrimer (AuG_1). Dissolution of the Au core leads to generation of large numbers of dendron radicals in a small volume, which underwent very fast coupling and addition reactions to form the Fréchet-type dendron nanoparticles (FDNs). The FDNs were found to be nearly monodisperse with an average size of 3 nm. NMR, TEM and MALDI-TOF analysis suggested that the FDNs are extremely dense organic structures made up of Fréchet-type dendrons. Although the FDNs do not contain any self-assembling motifs such as hydrogen bonding moieties, they exhibited time and concentration dependent morphological transformations, leading to formation of larger spherical aggregates and fibrous networks. The morphological transformations were probed using TEM, AFM and DLS studies. The self-assembly was found to be reversible. The morphological transformation of FDNs was exploited for encapsulation and on-demand release of guest molecules.

Introduction

Nanomaterials have received considerable attention in recent years because of the potential applications of these materials in several areas such as biomedicine,[1-4] optoelectronics,[5,6] sensing,[7,8] catalysis[9,10] etc. General methods available for the synthesis of nanomaterials include Brust - Schiffrin biphasic synthesis,[11] Stöbers method,[12] laser ablation technique,[13,14] microwave assisted synthesis,[15,16] microemulsion method,[17,18] sol-gel method[19,20] and template assisted synthesis.[21] Among the various methods mentioned above, the template assisted synthesis enables scientists to create nanomaterials with unique structures, which are otherwise difficult to prepare. This method consists of three steps: (i) preparation of the template, (ii) coating of the target material on the surface of the template and (iii) removal of the template by simple physical or chemical methods. A very attractive feature of this method is that one can use a variety of materials such as metals,[22,23] ceramics[24,25] or even soft polymers[26,27] as templates. The template material can also be in different forms such as zero-dimensional nanoparticles, one-dimensional nanowires or two- and three-dimensional hierarchical nanostructures. This method has been used for the synthesis of hollow[28,29] and hybrid[30,31] materials whose direct synthesis is not straightforward or thermodynamically favoured. Nanotubes,[32] nanowires[33], nanorods,[34] nanoparticle double helices[35] and half shell nanostructures[36] are few other novel structures prepared by this method.

Compared to their inorganic counterparts organic nanoparticles have been explored less although they have a wide range of potential applications. Except for a few examples,[37-41] most of the organic nanoparticles are prepared by emulsification or precipitation methods. Under these conditions, the organic nanoparticles are formed by non-covalent association of small organic molecules[42,43] or polymers.[44,45] Reports dealing with synthesis of robust, covalently cross-linked organic nano-assemblies are rare in the literature. Herein we report the use of a sacrificial template assisted strategy for synthesising Fréchet-type dendron based organic nanoparticles (FDNs) wherein the dendron units are covalently cross-linked to each other. To the best of our knowledge this is the first report on the synthesis of covalently cross-linked organic nanoparticles by template mediated synthesis.

Recently we have reported the synthesis and characterization of gold nanoparticle-cored dendrimers (AuG_1 NCD) with carbon-gold covalent bonds.[46] In the AuG_1 NCD the Fréchet-type dendrons (Scheme 1) are assembled on the surface of the gold nanoparticle in close proximity to each other. The FDNs described herein were prepared by dissolving away the

Journal of Materials Chemistry B Accepted Manuscript

gold core in AuG_1 NCD (TEM image of the Au NCD is given in Figure S1, Supporting Information (SI)). We envisioned that if we could somehow remove the gold core within a short time, then a large number of dendron radicals would be generated in a small volume as shown by $[D^{\bullet}]_n$ in Scheme 1. Nearly 130 dendrons would be attached to a 2.7 nm sized core in nanoparticle-cored G_1 dendrimer.[47] When the gold core is removed in a fast reaction, these dendron radicals are liberated into the small space where they undergo typical radical reactions such as radical-radical coupling and addition reactions with neighbouring dendrons, resulting in the formation of FDNs as shown in Scheme 1. In this paper we report the synthesis and characterization of the FDNs (which are also referred to as organic nanodots in this paper) using several experimental techniques. We observed that at high concentrations the FDNs can self-assemble into larger particles capable of guest encapsulation. Self-assembly and guest encapsulation properties of FDNs are also reported herein.

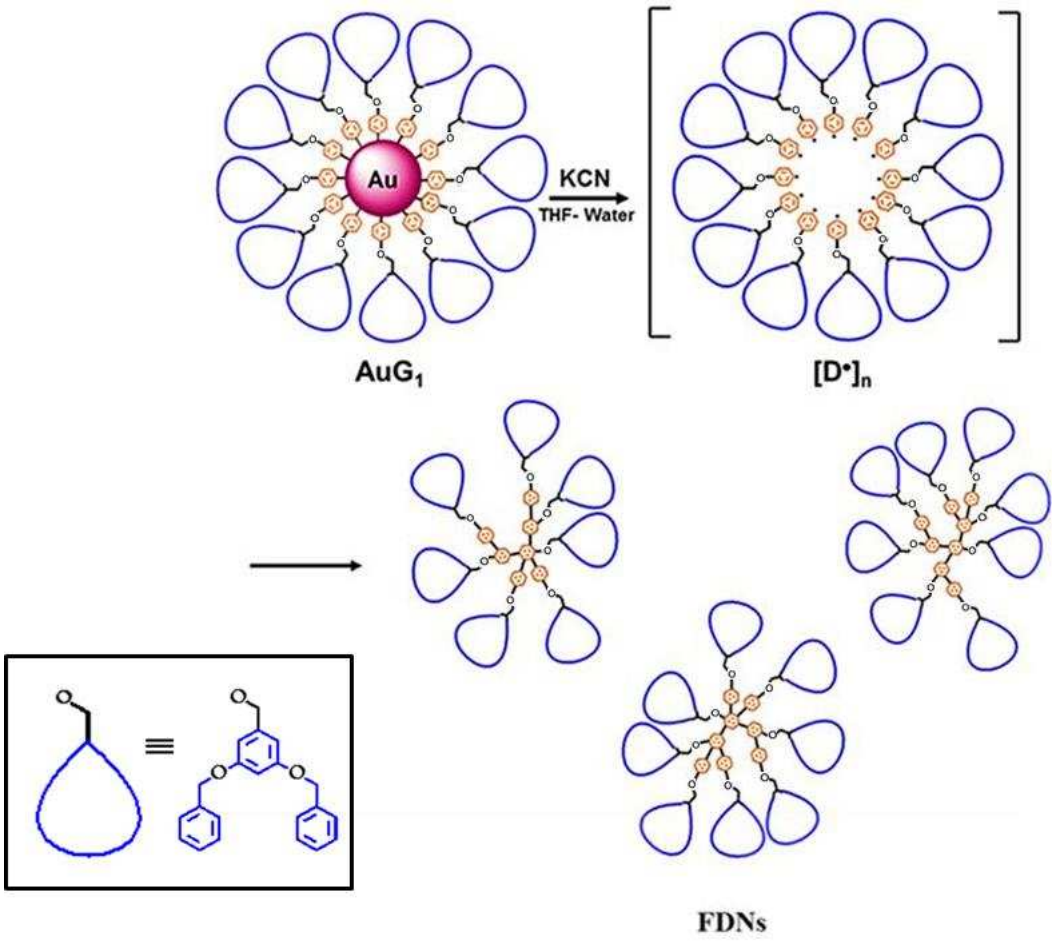

Scheme 1. Scheme for the synthesis of FDNs

Results and Discussion

Synthesis and Characterization of FDNs

The FDNs were prepared by etching away the Au core in AuG_1 NCD. In a typical reaction, an aqueous solution of potassium cyanide was mixed with a solution of the gold NCD in tetrahydrofuran. The color of the solution immediately changed from ruby red to brown. Completion of the reaction was confirmed by disappearance of the plasmonic band of gold nanoparticle at 520 nm (Figure S2, SI). Any exess amount of potassium cyanide present was washed off with copious amounts of water and the crude product was purified by repeated reprecipitation from dichloromethane-ether mixture. The total organic content in the AuG_1 NCD was 45% and yield of FDN was 40% (see experimental section) indicating that nearly 90% of the dendrons present in the NCD are retained in the FDNs. The FDNs thus prepared were soluble in acetone, THF and dichloromethane and insoluble in alcohols and ether (see Table ST1 in SI). We have characterized the FDNs using a variety of spectroscopic and microscopic techniques and the details are presented in the following sections.

In order to assess the molecular weight of FDNs, MALDI-TOF analysis was carried out and the spectrum

Journal of Materials Chemistry B Accepted Manuscript

obtained is shown in Figure S3, SI. The spectrum exhibited a maximum intense peak at 4914, which corresponds to twelve Fréchet-type dendron units (MW 4730) with an addition of 8 sodium ions. It is also possible that FDN can also enclose trapped solvent molecules. The tailing of the peak may be due to FDNs containing varying numbers of solvent molecules or small ions. Based on the MALDI-TOF mass spectrum we assumed that the FDNs are made up of approximately twelve dendron units and its average molecular weight is 4730 Da.

The transmission electron microscope (TEM) image of the FDN is shown in Figure 1. The TEM image shows nearly monodisperse particles having size of around 3 nm indicating that the radicals formed upon leaching of the Au core underwent rapid addition and coupling reactions as shown in Scheme 1 to generate very dense covalently cross-linked organic nanoparticles. Visualisation of dendrimers, except for metallodendrimers, using TEM is possible only with the assistance of staining agents or by using cryo-TEM, as the scattering power of dendrimers is insufficient for TEM imaging.[48] In the present case, the FDNs can be directly visualised in the TEM, implying that the dendron units are densely packed in the nanoparticle. The MALDI-TOF studies suggested that each FDN of 3 nm size, seen in the TEM image, is composed of nearly 12 dendron units. Considering the fact that the calculated end to end length of a dimer formed by the coupling of two dendron units is ~3 nm, the packing of 12 dendron units in a three dimensional 3 nm space is a strong indication of the densely packed nature of the FDNs formed.

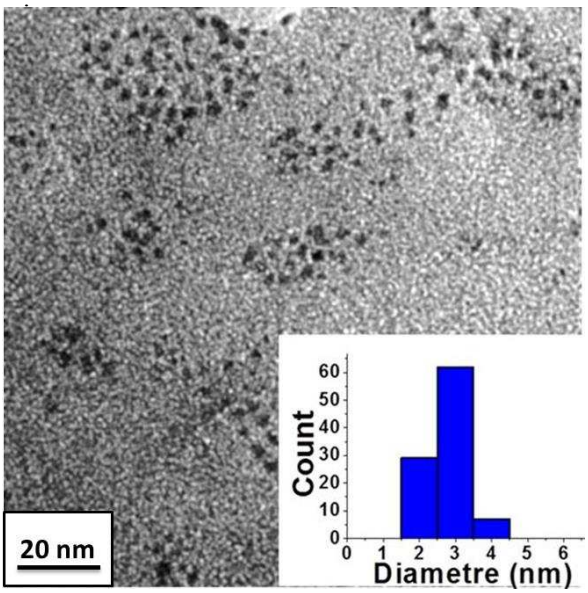

Fig. 1 TEM image of FDN: Inset - Core-size histograms for FDNs. TEM samples were prepared by drop casting 1.3×10^{-7} M FDN in acetone onto standard carbon-coated formvar films on copper grids (300 mesh) and drying in air for 2 days.

The energy dispersive X-ray (EDX) of the FDN (Figure S4, SI) did not show any peak corresponding to gold. The EDX spectrum showed peaks corresponding only to carbon, oxygen and copper (from the grid). The EDX spectrum thus confirms that the cyanide etching process has efficiently removed all the gold from the NCD and the FDN obtained is free of Au atoms

Dynamic light scattering (DLS) experiments (Figure S5, SI) of freshly prepared FDN samples show a number averaged mean particle size of about 3.4 nm. However, DLS is not a preferred method of choice for the characterization of particles of very small sizes such as the FDNs reported herein. Therefore, a more detailed discussion is not attempted here. It may however be noted that the particle size obtained by DLS is in good agreement with results from TEM analysis.

The FDNs were also examined by X-ray photoelectron spectroscopy (XPS). XPS studies are expected to provide information regarding the chemical environment of the core electrons in the material. The XPS survey spectrum (Figure S6a, SI) of the nanoparticle shows only two major peaks at 284.9 and 532.9 eV, which correspond to C1s and O1s core energy level positions, respectively. Furthermore, deconvoluting the C1s spectrum (Figure S6b, SI) gave three peaks at 284.6, 285.1 and 286.1 eV, which are attributed to C=C, C-H, and C-O bonds respectively. The O1s spectrum exhibits only one peak at 532.9, which corresponds to the ether linkage (C-O-C). The XPS spectrum did not show any peak corresponding to Au, further confirming the complete removal of the gold nanoparticle core in the etching process. XPS analysis thus indicates that the FDNs are composed of only poly(aryl ether) units.

The ^{1}H NMR spectrum (Figure S7, SI) of the FDNs shows four broad peaks at δ 7.3, 7.0, 6.5 and 5.0 ppm. The peaks at δ 7.3 and 6.5 correspond to aromatic protons and the peak at 5.0 ppm corresponds to -O-CH_2 protons of the Fréchet dendron. The dendron precursor (G_1- alcohol) also exhibited ^{1}H NMR signals around δ 7.3, 6.6 and 5.0 ppm. This shows that dendritic arms are not lost during the etching process. The peak at δ 7.0 ppm is assigned to the radical-bearing phenyl group which undergoes coupling reactions to give the FDN. Although this phenyl group originally contains four protons, some will be eliminated during radical coupling reactions. Dense or solid-like packing restricts or prevents free rotation of moieties within the FDNs resulting in large numbers of conformations for the aryl and CH_2 protons. NMR signals arise from each of the available conformations leading to broadening of the signal.[49,50]

^{13}C NMR spectrum of the FDN (Figure S8a, SI) is also broadened with peaks at δ 70.0, 101.5, 106.1, 127.5, 127.9, 128.5, 136.7, and 160.1 ppm. The spectrum was very similar to the ^{13}C NMR spectrum of AuG_1 NCD reported previously,[46] suggesting that the FDN is made up of the organic moieties present in Au-NCD. DEPT-135 ^{13}C NMR spectrum of the FDN material is shown in Figure S8b (SI).

Journal of Materials Chemistry B Accepted Manuscript

Disappearance of the peaks at δ 160.1 and 136.7 ppm in the DEPT-135 spectrum indicates that these peaks correspond to substituted phenyl ring carbons in the Fréchet-type G_1 dendron moiety. The signal at 70 ppm became negative in DEPT-135 spectrum confirming the presence of -CH_2 groups in the FDN. Detailed analysis of the ^{13}C spectrum was difficult due to broadening of the NMR signals.

IR spectrum of the material (Figure S9, SI) was similar to that of the precursor gold NCD[46] and featured methylene C-H stretching modes at 2870 and 2927 cm^{-1} and aromatic C-H vibration modes at 3030 and 3061 cm^{-1}. It also exhibited C=C breathing modes in the region 1400-1600 cm^{-1}. These features further confirm that FDNs are composed of organic residues of Au-NCDs and do not possess any other functional groups.

Thermal stability of the FDNs (Figure S10, SI) was measured using thermo gravimetric analysis. The FDNs were found to be stable up to 130 ^0C and decompose in the 130 – 650 ^0C range leaving a char yield of ~10%. Percentage char yield is reported to increase with increase in the degree of cross linking in polymers.[51,52] Thus the char yield of ~ 10% observed may be attributed to the cross-linking in FDN.

In this work FDNs were prepared by etching gold using cyanide ions. Gold can also be etched by reaction with KI/I_2 or aqua regia.[53,54] We have attempted to etch the gold core is AuG_1 NCD also and preliminary experiments showed that etching with aqua regia led to formation of FDNs with average diameter of 4.2 nm. Etching with KI/I_2 did not form FDNs. Details of these reactions will be reported elsewhere. IR, XPS and NMR data clearly showed that the FDNs formed do not have any functional groups other than the poly(aryl ether) moiety. TEM, NMR and TGA indicates that the FDNs formed are dense aggregates of poly(aryl ether) moieties heavily crosslinked to each other. These materials were formed as a result of rapid coupling and addition reactions of dendron radicals. Although dissolution of the Au core resulted in the release of large numbers of dendron radicals into a small volume (Scheme 1), the FDNs formed contained only ~12 dendron units suggesting that several FDNs are formed from one NCD. Since nearly 90% of dendrons are retained in the FDNs we conclude that only a small fraction of the dendron radicals escaped the cage as dimers or smaller oligomers. We have attempted to conduct the etching reaction in the presence of radical scavengers such as hydroquinone and *t*-butanol. Preliminary results indicated that radical scavengers inhibit the formation of FDNs, supporting our contention that FDNs are formed by radical reactions. We also attempted to synthesize FDNs from dendron radical precursors having a diazophenyl group at the focal point.[46] Reduction of the G_1- diazodendron with sodium borohydride yielded dendron radicals, which underwent addition and coupling reactions to give only dimers or low molecular weight oligomers containing 3-4 dendron residues. We conclude that formation of FDN requires fast generation of large numbers of dendron radicals within a small volume as shown in Scheme 1.

Self-Assembly of FDNs

Interestingly we observed that the FDNs exhibited concentration dependent size tunability and time dependent morphological transformations. A detailed investigation of the size and time dependent morphological changes of the FDNs were carried out in acetone solution using TEM, atomic force microscopy (AFM) and DLS. Similar morphological transformations are also seen in toluene and acetonitrile.

The TEM images of FDNs at three different concentrations are shown in Figure 2 (left panel). Figure 2 shows that size of the particles increases with increase in concentration. Particles in the size range 100-150 nm were obtained at a concentration of 1.3×10^{-6} M (Figure 2a). Upon increasing the concentration ten times (i.e. 1.3×10^{-5} M), particles in the size range 300-600 nm were obtained (Figure 2c). Upon increasing the concentration to 1.3×10^{-4} M, particles within the size range 800-1500 nm were obtained (Figure 2e). The concentration-dependent increase in size of the FDNs must be due to the aggregation of smaller particles. Presence of smaller nanoparticles along with larger ones in Figures 2c and 2e supports the above suggestion. Observations similar to this was reported previously in the case of peptide microvesicles.[55]

To get further insight into the topology of the FDNs, AFM studies were performed (Figure 2, right panel). At a concentration of 1.3×10^{-6} M, the particles exhibited diameter in the range of 100-150 nm and height in the range 2-3 nm (Figure 2b). At 1.3×10^{-5} M concentration, size range was 300-500 nm (Figure 2d). The heights of these particles were found to be in the range 10-12 nm. Particles with diameter in the range 700-1000 nm and height 300-350 nm were obtained at the high concentration of 1.3×10^{-4} M (Figure 2f). These results showed that upon increasing the concentration the height of the particles also increased substantially. For example, at a concentration of 1.3×10^{-6} M, the diameter to height ratio was 50:1 but at a higher concentration of 1.3×10^{-4} M, this ratio decreased to almost 2:1. This indicates that the particles undergo concentration-dependent multidimensional growth.

Journal of Materials Chemistry B Accepted Manuscript

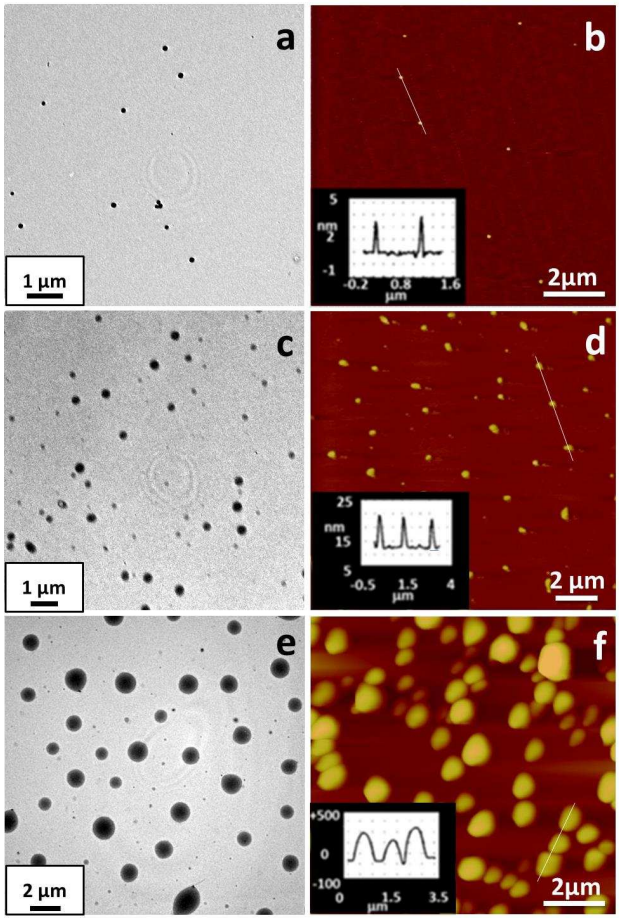

Fig. 2 TEM (a,c,e) and AFM (b,d,f) images of FDNs at various concentrations; 1.3×10^{-6} M (a and b), 1.3×10^{-5} M (c and d) 1.3×10^{-4} M (e and f). Inset (bottom left of b,d,f) - Height profile of respective images.

DLS measurements were found to be in close agreement with the TEM and AFM results (Figure S11, SI). When FDN concentration was 1.3×10^{-6} M, size distribution was found to be 90-140 nm, whereas a size distribution of 300-500 nm was obtained when concentration was increased to 1.3×10^{-5} M. Upon further increasing the concentration to 1.3×10^{-4} M, DLS experiment showed size distribution in the range 700-1300 nm. The correlograms of the particles formed at different concentrations of the FDN were found to be slightly distorted (Figure S11, SI) when compared to that reported for spherical particles suggesting that these particles are non-spherical in nature.

We observed that the FDNs undergo morphological transition from particles to fibrous networks over a period of 9 weeks at an optimal concentration of 1.3×10^{-6} M. This transition was monitored using TEM, AFM and DLS. Figure 3a-d shows the TEM images of the sample drop casted at different time intervals. Figure 3a shows that the particles are fusing with each other through the development of a neck (see inset in Figure 3b and Figure S12, SI for more images). TEM images taken after three

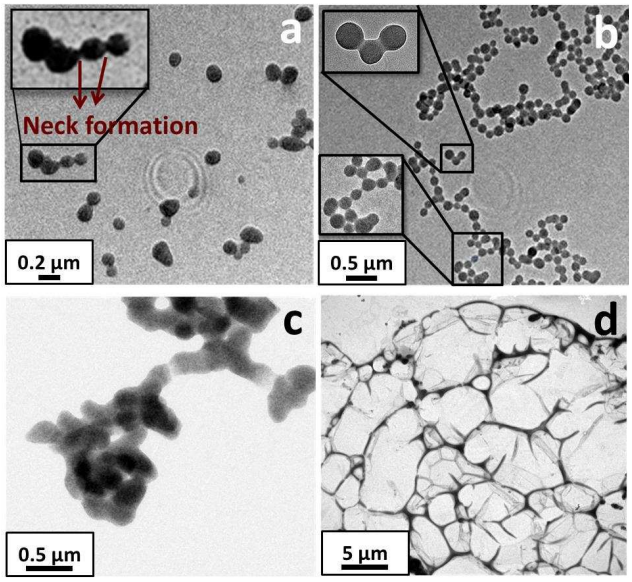

Fig. 3 TEM images of FDN (1.3×10^{-6} M) as a function of time; after 1 week (a) 3 weeks (b), 6 weeks (c) and 9 weeks (d). Inset (a,b) – zoomed in image of particles fusing together by neck formation.

weeks showed joining together of large number of particles forming a network (Figure 3b). In Figure 3c we can observe the coalescing of interlinked particles in to fibrous assemblies. Denser interwoven fibrous networks shown in Figure 3d were seen at the end of 9 weeks.

AFM studies also confirm the time-dependent particle to fibrous network formation. Figure 4 shows the AFM image of the sample drop casted at different time periods. Figure 4a clearly shows the fusing of the particles to form network of fibres. The heights of the fibres were found to be in the range 10-30 nm. DLS experiments were also performed to monitor the time-dependent particle to fibre transition. The diameter of the aggregates increased from the range 100-140 nm to 420-530 nm and the

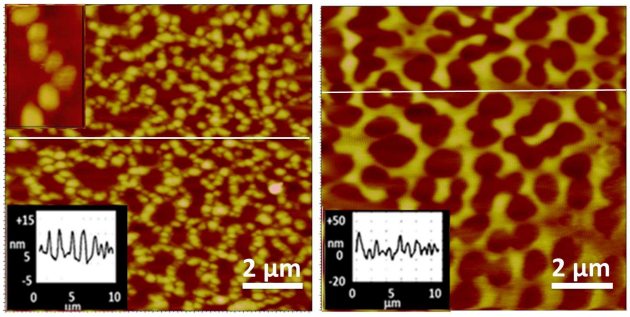

Fig. 4 AFM images of FDN (1.3×10^{-6} M) as a function of time; after 6 weeks (a) and after 9 weeks (b). Inset (top left in a) – zoomed in image of particles fusing together; Inset (bottom left) - Height profile of respective images.

Journal of Materials Chemistry B Accepted Manuscript

correlogram was further disrupted (Figure S13, SI) indicating the transformation from particle to fibre.[56]

We observed that the larger aggregates shown in Figure 2e,f can be broken down into smaller particles upon sonication for a few minutes. The larger fibrous structures could also be broken down to particles in the 100-900 nm size range (Figure 5a) and further to nanodots in the size range of 2-5 nm (Figure 5b) by ultrasound sonication. The breaking down of the self-assembled structures on sonication indicates that the FDNs are held together by weak forces. o

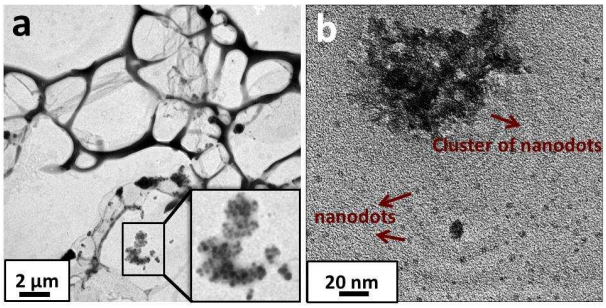

Fig. 5 TEM images of (a) fibre-network after sonication for 15 min; Inset-zoomed in image of particles formed on sonication, (b) FDNs formed on further sonication (60 min).

As evidenced by the TEM data, the nanoparticles formed initially by leaching of the gold core have dimensions in the range of 2-3 nm. It is obvious that the concentration-dependent self-assembly to form large disc-like particles and the time-dependent self-assembly leading to formation of fibrous networks result from the aggregation of the smaller nanodots. It is interesting to note that the FDNs undergo morphological transitions in the absence of any conventional self-assembling motifs like hydrogen bonding, electrostatic, or dipole-dipole types of interactions. In the absence of any such interactions it is only reasonable to assume that association of the nanodots into larger particles occur through intercalation of the phenyl rings present on the periphery of the nanoparticle. The intercalated phenyl groups may participate in π-π interactions leading to stabilization of the larger particles. The overall transition can be schematically represented as shown in Scheme 2. At higher concentrations the FDNs aggregate to form larger sized particles with disc-like morphology. These aggregates can also undergo time-dependent self-assembly to give fibrous networks. The self-assembled structures could be reverted back to the FDNs by ultrasound sonication.

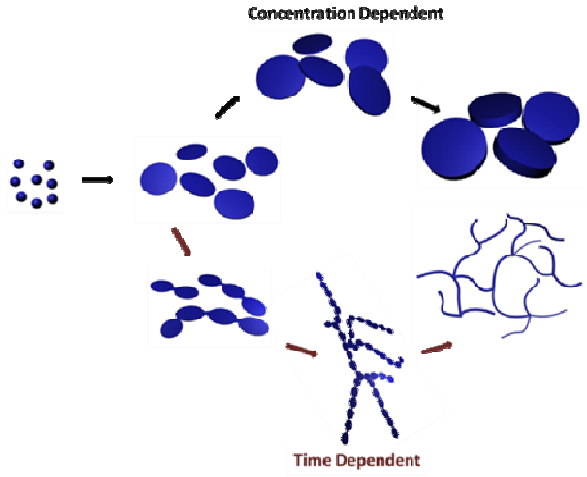

Scheme 2 Concentration dependent and time-dependent self-assembly of FDNs.

Guest encapsulation and release by FDN

Supramolecular systems capable of encapsulation and stimuli responsive release of guest molecules are of great demand as they are potential candidates for controlled drug release.[57-61] We observed that FDNs can encapsulate and release small organic molecules. Rhodamine 6G (R6G) was selected for this study and encapsulation was effected by solid/liquid phase transfer method.[62,63] R6G is insoluble in toluene but can be captured into toluene in the presence of dissolved FDN. Upon stirring a FDN solution in toluene (1×10^{-4} M, 5 mL) with powdered R6G (1 mg) for 12 h, the color of the toluene layer changed from light brown to pink (Inset of Figure S14, SI) indicating the dissolution of R6G in the toluene layer. Figure S14 (SI) also shows the fluorescence excitation and emission spectra of the toluene layer and the spectra are identified as due to R6G. Since R6G is insoluble in toluene, we believe that the R6G molecules are present in FDN-encapsulated form in the toluene solution. Upon evaporation of toluene solvent the R6G encapsulated FDN (designated as R6G@FDN) was obtained as a dry powder. A control experiment was performed wherein solid R6G was stirred in toluene in the absence of FDNs. In this case R6G was not partitioned into the toluene layer as evidenced by absence of pink colour and characteristic R6G fluorescence.

FDNs are very dense organic structures and encapsulation of R6G inside FDN structures shown in Scheme 1 would be difficult. At 1×10^{-4} M concentration, the FDNs are present as large aggregates of ~1 µm diameter with each aggregate containing several hundred FDNs. These aggregates can accommodate the R6G molecules in the interstitial space between the FDNs leading to formation of R6G@FDN. This suggests that the breaking of the aggregates into smaller particles would also lead to release of R6G molecules. We actually observed that the R6G@FDN releases R6G into

Journal of Materials Chemistry B Accepted Manuscript

water when sonicated or heated. We have monitored R6G release into aqueous solution at three temperatures (40 ˚C, 60 ˚C and 80 ˚C) and also as a function of ultrasound sonication time at room temperature and the results are presented in Figure 6. At 80 ˚C nearly 75% of R6G was released into aqueous solution in 6 h. Only 24% of the dye was released when temperature was maintained at 60 ˚C. Less than 2% of

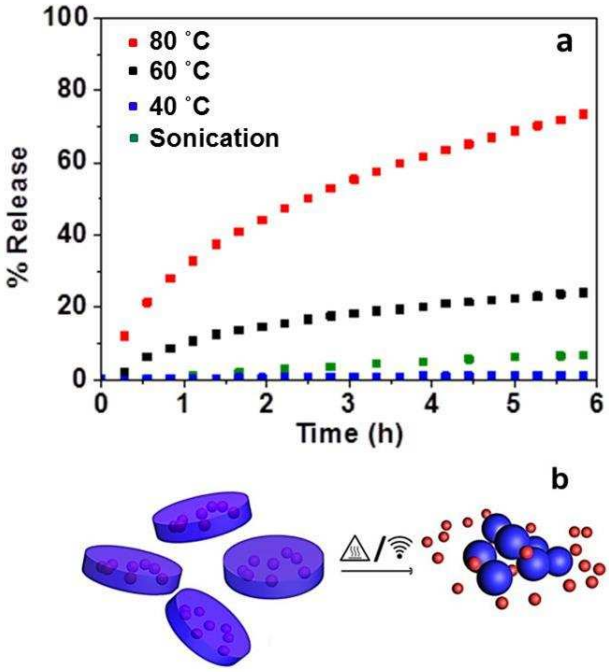

Fig. 6 (a) Percentage dye release into water as a function of time for R6G@FDN. (b) Schematic representation of R6G@FDN breaking into smaller aggregates and concomitant release of R6G on application of heat or ultrasound.

R6G was released by heating at 40 ^{0}C for 6 h. Ultrasound sonication of the system resulted in the release of 7% of the dye at the end of 6 h. De-aggregation of self-assembled nanostructures is well documented in the literature.[64] At 80 ^{0}C, rates of de-aggregation and release of R6G are much faster compared to the rates of these processes at lower temperatures or under ultrasound sonication conditions. At 40 ^{0}C the rate of release of the dye is very slow. Thus depending on the applied stimulus controlled release of the encapsulated guest is possible making this system suitable for on-demand release of guest molecules

R6G intake and release by FDN solution can be observed using confocal microscope. Figure 7a shows the confocal fluorescence image from R6G captured FDN solution. Bright green fluorescence spots indicated that the FDNs are loaded with R6G. Figure 7b is the confocal image obtained from the FDN solution after dye release. There are no fluorescence spots indicating that the dye was released completely from the FDNs. This study also showed that fluorophore encapsulated FDN may also find application in fluorescence imaging.

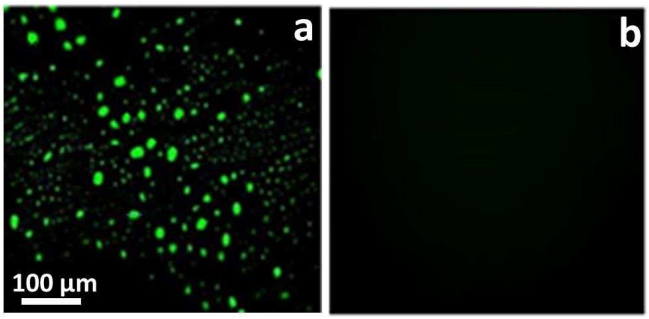

Fig. 7 Confocal microscopic images of FDNs (a) after encapsulation of R6G and (b) after release of R6G

Conclusion

In conclusion, we report the sacrificial-template assisted synthesis and characterization of a new dendron based nanodot from AuG_1 NCD containing Au-C covalent bonds. Spectroscopic studies suggest that the FDNs are formed by the fast coupling and addition reactions of the G_1 dendron units, which were formed when the Au core is leached out in a fast reaction. NMR, IR, EDX and XPS data proved beyond doubt that the Au core was completely removed and the FDNs are composed entirely of aryl ether dendron moieties. TGA measurements showed that the FDNs are robust and stable up to 130 ^{0}C. These nanoparticles further underwent concentration and time dependent self-assembly to form bigger disc-like particles and fibrous networks, respectively, which were reversible by ultrasound sonication. The morphological transformations were probed using TEM, AFM and DLS studies. We have further shown that FDNs can encapsulate guest molecules within their structre and these can be released upon application of suitable stimuli. These systems may have potential applications in controlled release and fluorescence imaging.

Experimental section

Materials and methods

AuG_1 NCD was synthesized by a procedure reported before.[46] Potassium cyanide and deuterated solvents were purchased from Aldrich and used as received. Solvents such as acetone, toluene, dichloromethane, tetrahydrofuran etc. were obtained from MERCK and used as received. For the spectroscopic studies spectroscopic grade solvents from MERCK were used. Absorption spectra were obtained using a Shimadzu 3101PC UV/Vis-NIR scanning spectrophotometer. Emission spectra were recorded on a SPEX-Fluorolog FL-1039 spectrofluorimeter. HRTEM images were obtained with a 200 kV FEI Tecnai 30G2S-Twin transmission electron microscope. Samples for TEM analysis were prepared by drop casting solutions of FDN in acetone onto standard carbon-coated Formvar films on copper grids (300 mesh) and drying in air for 2 days. Atomic Force Microscopy images

Journal of Materials Chemistry B Accepted Manuscript

were recorded under ambient conditions using a NTEGRA (NT-MDT) operating with a tapping mode regime. Micro-fabricated TiN cantilever tips (NSG10) with a resonance frequency of 299 kHz and a spring constant of 20-80 Nm^{-1} were used. AFM section analysis was done offline. Samples for the imaging were prepared by drop casting the solution on freshly cleaved mica surface at the required concentrations at ambient conditions. DLS analyses were carried out with a Zetasizer Nano S from Malvern Instruments at 25 ^{0}C. The measurements were performed after the samples were thoroughly mixed and equilibrated for 2 min. The average hydrodynamic radii were calculated from Stork-Einstein equation $R_h = kBT/6\pi\eta D$. X-ray Photoelectron Spectroscopic (XPS) measurements were performed using a commercially available X-ray photoemission spectrometer (Omicron Nanotechnology, Germany) using Al Kα (1486.7 eV) as X-ray source operating at 100 watts. General scans and core-level spectra were acquired with 1 eV and 50 eV pass energy, respectively. Spectral background (Shirely) de-convolution was done by using Fityk software. FTIR spectra were recorded with a Shimadzu IR Prestige 21 spectrometer.^{1}H NMR and ^{13}C spectra were collected at 500 and 125 MHz, respectively, on a Bruker Avance DPX spectrometer. MALDI-TOF mass spectrometry was performed on an UltrafleXtreme instrument with trans-indoleacrylic acid as the matrix. Samples for MALDI-TOF analysis were prepared by mixing tetrahydrofuran solutions of FDN and the matrix in 1: 3 ratio. TGA experiments were performed using a Perkin–Elmer Pyris Diamond TG/DTA analyser under nitrogen atmosphere at a heating rate of 10 °C/min. Fluorescence imaging was carried out (Ex. 490 nm; Em. 550 nm) using a Spinning disk fluorescent microscope (BD Pathway™Bioimager system, USA).

Synthesis of FDNs

AuG_1 (50 mg) was dissolved in tetrahydrofuran (5 mL) and added to KCN (2×10^{-2} M) in water (50 mL) at a fast rate. The color of the solution changed from ruby red to brown within ~5 minutes. The reaction mixture was allowed to stir for 30 min. It was then added to excess water and extracted into CH_2Cl_2. The CH_2Cl_2 layer was washed with water several times to remove all the CN- ions. The organic layer was separated, dried over sodium sulphate and concentrated in vacuum. The crude product thus obtained (20 mg) was dissolved in minimum amount of CH_2Cl_2 and re-precipitated with ether. This procedure was repeated several times for the purification of the product**.**

Encapsulation and Release of R6G by FDNs

R6G (1 mg, 2 mmol) was added to a toluene solution of FDN (10^{-4} M) and the suspension was stirred for 12 h. Any undissolved dye was removed by ultracentrifugation and filtration. The toluene layer was then separated and its emission was measured. R6G@FDN was prepared by evaporating off toluene. The solid powder obtained was further dried in vacuum to remove any trace amount of solvent. The amount of R6G encapsulated by FDN was quantified by refluxing R6G@FDN in water (0.4 mg/mL) for 6h and measuring the absorbance of the water layer at 525 nm. For the R6G release studies R6G@FDN (1 mg) was suspended in water (2 mL) and heated at 40 - 80 ^{o}C or sonicated. Percentage release was determined from the absorbance of the aqueous solution at 525 nm as a function of time.

Acknowledgment

We gratefully acknowledge the CSIR and the Network project CSC0125 for financial support. We also thank JNCASR for the XPS spectra and RGCB, Trivandrum for MALDI-TOF analysis.

Notes and References

Photosciences and Photonics Section, Chemical Sciences and Technology Division, CSIR-National Institute for Interdisciplinary Science and Technology, Council of Scientific and Industrial Research (CSIR), Trivandrum-695019 (India).
E-mail:gopidaskr@rediffmail.com

Electronic Supplementary Information (ESI) available: UV-Visible absorption spectra of FDN and AuG_1, ^{13}C, DEPT-135 ^{13}C NMR, DLS, IR, spectra and thermogram of FDNs, DLS spectra showing concentration and time dependent morphological changes of FDN, TEM image showing particles fusing together, excitation and emission spectra of R6G@FDN. See DOI: 10.1039/b000000x/

1. E. C. Dreaden, A. M. Alkilany, X. Huang, C. J. Murphy and M. A. El-Sayed, *Chem. Soc. Rev.,* 2012, **41**, 2740.
2. G. Y. Tonga, K. Saha and V. M. Rotello, *Adv. Mater.,* 2014, **26**, 359.
3. V. Voliani, G. Signore, O. Vittorio, P. Faraci, S. Luin, J. Peréz-Prieto and F. Beltram, *J. Mater. Chem. B*, 2013, **1**, 4225.
4. V. Voliani, F. Ricci, S. Luin and F. Beltram *J. Mater. Chem.*, 2012, **22**, 14487.
5. D. V. Talapin, J.-S. Lee, M. V. Kovalenko and E. V. Shevchenko, *Chem. Rev.,* 2010, **110**, 389.
6. H. Choi, S.-J. Ko, Y. Choi, P. Joo, T. Kim, B. R. Lee, J.-W. Jung, H. J. Choi, M. Cha, J.-R. Jeong, I.-W. Hwang, M. H. Song, B.-S. Kim and J. Y. Kim, *Nature Photon.,* 2013, **7**, 732.
7. K. Saha, S. S. Agasti, C. Kim, X. Li and V. M. Rotello, *Chem. Rev.,* 2012, **112**, 2739.
8. J. C. Claussen, A. Kumar, D. B. Jaroch, M. H. Khawaja, A. B. Hibbard, D. M. Porterfield and T. S. Fisher, *Adv. Funct. Mater.,* 2012, **22**, 3399.
9. A. Roucoux, J. Schulz, H. Patin, *Chem. Rev.,* 2002, **102**, 3757.
10. V. K. R. Kumar, S. Krishnakumar and K. R. Gopidas, *Eur. J. Org. Chem.,* 2012, 3447.
11. M. Brust, M. Walker, D. Bethell, D. J. Schiffrin and R. Whyman, *J. Chem. Soc., Chem. Commun.,* 1994, 801.
12. W. Stöber, A. Fink and E. Bohn, *J. Colloid Interface Sci.,* 1968, **26**, 62.
13. S. Barcikowski and G. Compagnini, *Phys. Chem. Chem. Phys.,* 2013, **15**, 3022.
14. H. Wender, M. L. Andreazza, R. R. B. Correia, S. R. Teixeira and J. Dupont, *Nanoscale,* 2011, **3**, 1240.
15. G. A. Kahrilas, L. M. Wally, S. J. Fredrick, M. Hiskey, A. L. Prieto and J. E. Owens, *ACS Sustainable Chem. Eng.,* 2014, **2**, 367.
16. I. Bilecka and M. Niederberger, *Nanoscale,* 2010, **2**, 1358.
17. A. K. Ganguli, A. Ganguly and S. Vaidya, *Chem. Soc. Rev.,* 2010, **39**, 474.
18. J. Eastoe, M. Hollamby and L. Hudson, *Adv. Colloid Interface Sci.,* 2006, **128**, 5.
19. R. Sui and P. Charpentier, *Chem. Rev.,* 2012, **112**, 3057.

Journal of Materials Chemistry B Accepted Manuscript

20. P. K. Deheri, V. Swaminathan, S. D. Bhame, Z. Liu and R. V. Ramanujan, *Chem. Mater.,* 2010, **22**, 6509.
21. Y. Liu, J. Goebl and Y. Yin, *Chem. Soc. Rev.,* 2013, **42**, 2610-2653.
22. M. Chen and L. Gao, *Inorg. Chem.,* 2006, **45**, 5145.
23. A. Sanchez-Iglesias, M. Grzelczak, B. Rodríguez-González, R. A. Alvarez-Puebla, L. M. Liz-Marzán and N. A. Kotov, *Langmuir,* 2009, **25**, 11431.
24. E. M. Saurer, R. M. Flessner, M. E. Buck and D. M. Lynn, *J. Mater. Chem.,* 2011, **21**, 1736.
25. F. I. Dar, S. Habouti, R. Minch, M. Dietze and M. Es-Souni, *J. Mater. Chem.,* 2012, **22**, 8671.
26. A. Chatzipavlidis, P. Bilalis, E. K. Efthimiadou, N. Boukos and G. C. Kordas, *Langmuir,* 2011, **27**, 8478.
27. W. Yuan, Z. Lu, H. Wang and C. M. Li, *Phys. Chem. Chem. Phys.,* 2013, **15**, 15499.
28. M. Wu, S. A. O'Neill, L. C. Brousseau, W. P. McConnell, D. A. Shultz, R. J. Linderman and D. L. Feldheim, *Chem. Commun.,* 2000, 775.
29. S. Beyer, J. Bai, A. M. Blocki, C. Kantak, Q. Xue, M. Raghunath and D. Trau, *Soft Matter,* 2012, **8**, 2760.
30. F. Caruso, R. A. Caruso and H. Mohwald, *Science,* 1998, **282**, 1111.
31. H. Zhao, J. Yang, L. Wang, C. Tian, B. Jiang and H. Fu, *Chem. Commun.,* 2011, **47**, 2014.
32. R. Li, Y.-P. Yuan, L.-G. Qiu, W. Zhang and J.-F. Zhu, *Small,* 2011, **8**, 225.
33. L. Qin, S. Park, L. Huang and C. A. Mirkin, *Science,* 2005, **309**, 113.
34. W. Han, S. Fan, Q. Li and Y. Hu, *Science,* 1997, **277**, 1287.
35. C.-L. Chen, P. Zhang and N. L. Rosi, *J. Am. Chem. Soc.,* 2008, **130**, 13555.
36. J. C. Love, B. D. Gates, D. B. Wolfe, K. E. Paul and G. M. Whitesides, *Nano Lett.,* 2002, **2**, 891.
37. A. Tuteja, M. E. Mackay, C. J. Hawker, B. V. Horn and D. L. Ho, *J. Polym. Sci., Part B: Polym. Phys.,* 2006, **44**, 1930.
38. X. Zhang, X. Zhang, B. Yang, J. Hui, M. Liu, S. Liu, Z. Chi, S. Liu, J. Xu and Y. Wei, *J. Mater. Chem. C,* 2014, **2**, 816.
39. X. Zhang, X. Zhang, B. Yang, J. Hui, M. Liu, Z. Chi, S. Liu, J. Xu and Y. Wei, *Polymer Chem,.* 2014, **5**, 683.
40. S. C. Zimmerman, J. R. Quinn, E. Burakowska and R. Haag, *Angew. Chem. Int. Ed.,* 2007, **46**, 8164.
41. E. Burakowska, S. C. Zimmerman and R. Haag, *Small,* 2009, **5**, 2199.
42. A. Kaeser and A. P. H. J. Schenning, *Adv. Mater.,* 2010, **22**, 2985.
43. D. Horn and J. Rieger, *Angew. Chem. Int. Ed.,* 2001, **40**, 4330.
44. D. Tuncel and H. V. Demir, *Nanoscale,* 2010, **2**, 484.
45. T. S. Kale, A. Klaikherd, B. Popere and S. Thayumanavan, *Langmuir,* 2009, **25**, 9660.
46. V. K. R. Kumar and K. R. Gopidas, *Chem. Asian J.,* 2010, **5**, 887.
47. V. K. R. Kumar and K. R. Gopidas, *Tetrahedron Lett.,* 2011, **52**, 3102.
48. F. Vögtle, G. Richardt and N. Werner, WILEY-VCH Verlag GmbH & Co. KGaA, Weinheim, 2009, 275.
49. K.-M. Lee, W.-Y. Cheng, C.-Y. Chen, J.-J. Shyue, C.-C. Nieh, C.-F. Chou, J.-R. Lee, Y.-Y. Lee, C.-Y. Cheng, S. Y. Chang, T. C. Yang, M.-C. Cheng and B.-Y. Lin, *Nature Commun.,* 2013, **4**, 1544.
50. M. S. Wendland and S. C. Zimmerman, *J. Am. Chem. Soc,.* 1999, **121**, 1389.
51. Y. S. Ye, Y. J. Huang, F. C. Chang, Z. G. Xuea and X. L. Xie, *Polymer Chem.,* 2014, **5**, 2863.
52. M. Trigo-López, J. L. Barrio-Manso, F. Serna, F. C. García and J. M. García, *Macromol. Chem. Phys.,* 2013, **214**, 2231.
53. C. Boyer, M. R. Whittaker, C. Nouvel, and T. P. Davis, Macromolecules 2010, **43**, 1792.
54. L. Sun, R. M. Crooks and V. Chechik, *Chem. Commun.*, 2001, 359.
55. S. Maity, P. Jana, S. K. Maity and D. Haldar, *Langmuir,* 2011, **27**, 3835.
56. S. Mahesh, A. Gopal, R. Thirumalai and A. Ajayaghosh, *J. Am. Chem. Soc.,* 2012, **134**, 7227.
57. J. Zhuang, M. R. Gordon, J. Ventura, L. Li and S. Thayumanavan *Chem. Soc. Rev.,* 2013, **42**, 7421.
58. J. Zhang, R. J. Coulston, S. T. Jones, J. Geng, O. A. Scherman, C. Abell, *Science,* 2012, **335**, 690.
59. L. -L. Li, J. -H. Xu, G. -B. Qi, X. Zhao, F. Yu and H. Wang, *ACS Nano,* 2014, **8**, 4975.
60. W. Chen and J. Du, *Sci. Rep.*, 2013, **3**, 2162.
61. S. Biswas, K. Kinbara, T. Niwa, H. Taguchi, N. Ishii, S. Watanabe, K. Miyata, K. Kataoka and T. Aida, *Nature Chem.,* 2013, **5**, 613.
62. Y. Kitajyo, Y. Nawa, M. Tamaki, H. Tani, K. Takahashi, H. Kaga, T. Satoh and T. Kakuchi, *Polymer,* 2007, **48**, 4683.
63. T. Satoh, *Soft Matter*, 2009, **5**, 1972.
64. U. Mayerhöffer and F. Würthner, *Chem. Sci.*, 2012, **3**, 1215.

Journal of Materials Chemistry B Accepted Manuscript

Table of contents

Organic Nanodots

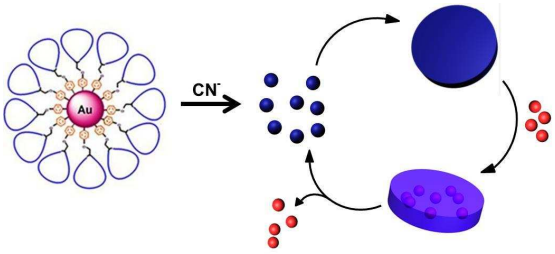

Novel Fréchet-type dendron based organic nanodots exhibiting stimuli responsive reversible morphological transformation have been synthesized by a one-pot reaction which involve etching off the gold core of a first generation gold nanoparticle cored dendrimer. The self-assembled FDNs can be utilized for encapsulation and on-demand release of guests.

Journal of Materials Chemistry B Accepted Manuscript